CHAPTER V

KRYTOX-MONTMORILLONITE-NAFION® NANOCOMPOSITE MEMBRANE FOR EFFECTIVE METHANOL CROSSOVER REDUCTION IN DMFCs

Abstract

Nafion® and Montmorillonite (MMT) functionalized with Krytox nanocomposite membrane (Krytox-MMT-Nafion®) is proposed for DMFC applications. The nanocomposite is obtained with good compatibility between MMT and Nafion® via the function of Nafion®-like polymer chain namely Krytox 157 FSL. The MMT layers are exfoliated with Nafion® polymer matrices and show homogeneity as confirmed by XRD and SEM. The AFM micrographs clarify the successful MMT clay dispersion all over the nanocomposite membrane. The thermogravimetric analysis exhibits the improvement in water retention and thermal resistance as compared to Nafion® membrane. The membranes perform for more than 50 % reduction in the permeation of methanol in 10 %(v/v) solution at either room temperature or as high as 60 °C. The Arrhenius plot suggests the lower activation energy for proton migration in the Krytox-MMT-Nafion® membranes than in the Nafion® membrane under Grotthus mechanism.

Keywords: Nafion®; Montmorillnite; Composite membrane; Low methanol crossover; DMFCs

1. Introduction

Direct methanol fuel cells (DMFCs) have received much attention as an alternative energy resource for wide applications especially for portable power sources since its liquid-fuelled system is an easy manipulation and low environmental impact. Moreover, they promise high energy efficiency because of no power consumption for fuel reforming and gas treatment processes [1-4]. Although DMFCs accomplish several benefits, their efficiency is substantially affected by two technical problems. One is the low catalytic activity for methanol oxidation at anode. The other is the methanol crossover through electrolyte membrane generating a

mixed potential at cathode and causing to a lower overall voltage performance as well as loss of fuel [5].

A perfluorosulfonic acid membrane (PFSA), such as Nafion® membrane is well known as a conventional proton exchange membrane in DMFC system due to its electro-chemical, mechanical and thermal stability together with high proton conductivity [6]. However, it cannot fulfill the requirement to be an effective barrier for methanol permeation. For instance, there is almost 40 % of methanol fuel loss across PFSA membrane even at low methanol concentration [7].

Therefore, many research efforts are mainly focused on the membrane development to reduce methanol crossover with favorable proton conductivity [8-10]. Owning to the excellent proton conductivity of Nafion® membrane, a number of studies have aimed to reduce its methanol permeability via the composite system by incorporating inorganic hybrid materials, such as organosilicate [2, 15, 16], titanium oxide [4, 17], calcium hydroxyphosphate and calcium phosphate [6, 13], silicon oxide either with or without modification [11, 12] and zirconium/titanium phosphate [14] into Nafion® by means of: (i) additive-dispersed solution casting [6, 13, 16, 18]; (ii) sol-gel reaction [3, 15]; (iii) spin-coating [17]; and (iv) plasma deposition [2]. Among several inorganic hybrid materials, montmorillonite (MMT) is accepted as an excellent barrier for the permeation of small molecules [19]. It is reported that only 5 wt.% of MMT incorporated into the polymer membrane contributes the reduction of methanol crossover as high as 40 %[5]. Jung et al. [9] prepared the composite membranes of Nafion®/MMT and Nafion®/dodecylamine-modified MMT (m-MMT) by direct melt injection. The methanol crossover values of the composite membranes were lower than that of pristine Nafion® membrane and decreased with the increases of MMT and m-MMT loading content. However, the reduction of methanol permeability for both composite membranes of Nafion® with either MMT or m-MMT was similar. This might be due to the poor dispersion of MMT in the Nafion® polymer matrices even though it was modified with organic salt. It can be expected that the exfoliated Nafion®-MMT nanocomposite is another challenge to improve the methanol crossover reduction. Song et al. [8] reported that the stacked-sheeted structure of the clay effectively provides high barrier property as well as thermal stability when the gallery of clay was exfoliated in the polymer matrices as

evidenced from the Nafion® and organically treated MMT clays (Closite 10A) solution casted membranes. Based on the nanoclay exfoliation, the tortuosity providing a longer diffusive path for permeating molecules causes the reduction in permeability [20].

In the previous study [21], we optimized the homogeneous Nafion®/silica composite membrane. Based on a "like-dissolves-like" concept, nanoparticulated silica (fumed silica) was functionalized with a type of fluorocarbon polymer, i.e., Krytox 157 FSL (carboxylic acid terminated perfluoropolyether, Scheme 5.1), and blended with Nafion® solution to obtain the miscibility of silica and Nafion® provided from the similar structure between Krytox and Nafion®. Our results, especially the good silica particle dispersion on Nafion® polymer matrices with an increase in thermal stability as well as an improvement of proton conductivity at elevated temperature brings us the next step of the work. Here, we propose the modification of silicate layered MMT with Krytox using the silane coupling agent to expect for the exfoliated nanocomposite structured membrane. The present article shows the steps of Krytox-MMT-Nafion® membrane preparation, the structural characterization, morphology, methanol permeability, thermal stability, water uptaking including the proton conductivity to clarify how exfoliated nanocomposite induces an effective methanol crossover reduction system.

2. Experimental

2.1. Materials

A 5 wt.% Nafion® solution in aliphatic alcohol was purchased from Aldrich, Germany. (3-Aminopropyl)triethoxysilane was obtained from Fluka, Switzerland. Krytox 157 FSL (carboxylic acid terminated perfluoropolyether) was purchased from DuPont, USA. A water conjugating agent (WSC), 1-(3-dimethylaminopropyl)-3-ethyl carbodiimide hydrochloride 98 %, was purchased from Acros, Belgium. Dimethylacetamide was bought from Merck KGaA, Germany. Sodium-montmorillonite (Na^+-MMT) namely Cloisite Na^+ was the product of Southern Clay Product, Inc., USA. All chemicals were used without further purification.

2.2. Preparation of Krytox-MMT-Nafion® composite membrane

Na^+-montmorillonite (MMT) (1.0062 g) was homogeneously dispersed into 75 % ethanol solution (200 ml) under vigorous stirring for 2 h. The hydrolyzed (3-aminopropyl)triethoxysilane, **1** (0.6 ml), prepared as shown in Step 1, was added into the MMT-ethanol suspension. The mixture was refluxed at 80 °C for 24 h, filtered and washed several times with distilled water to obtain aminosilane-functionalized MMT, **2** (Step 2). Compound **2** was stirred with WSC (0.7852 g, 4.0963×10^{-3} mol) in 250 ml of 75 % ethanol solution at room temperature for 6 h. Krytox 157 FSL (6.827 g, 2.7308×10^{-3} mol) was mixed with the molar ratio of Krytox: aminosilane: WSC 1:1:1.5. The mixture was vigorously stirred at room temperature for 24 h to obtain Krytox-funtionalized MMT, **3** (Step 3). Nafion® 5 wt. % (15 ml) in aliphatic alcohol solution was mixed with **3** for 2.5 and 5 wt.% in dimethylacetamide (15 ml) for 2 days and sonicated at ambient temperature for 1 h to obtain two types of the homogeneous hybrid solutions (Step 4).

Scheme 5.1 Krytox-Montmorillonite-Nafion® hybrid material preparation

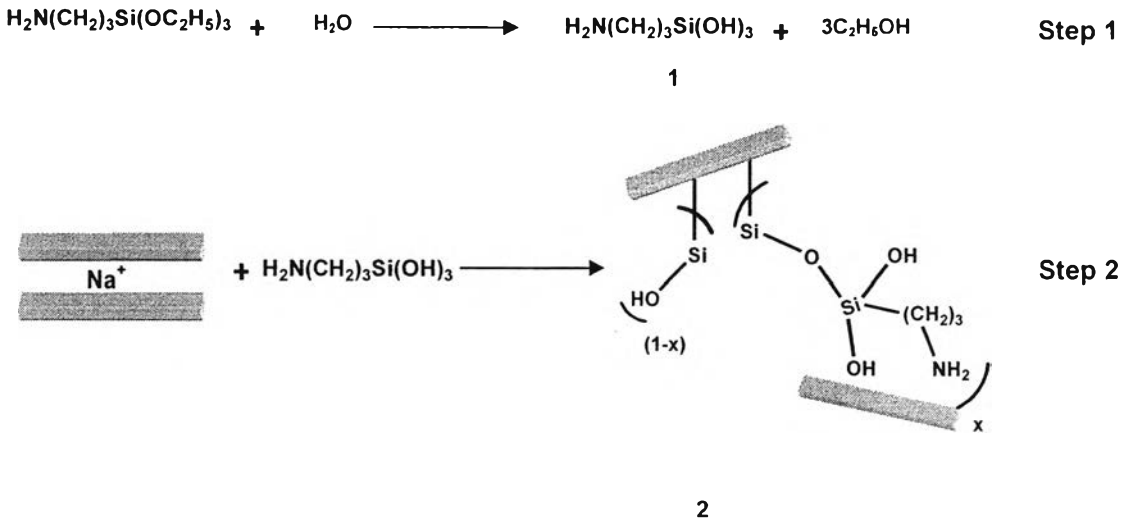

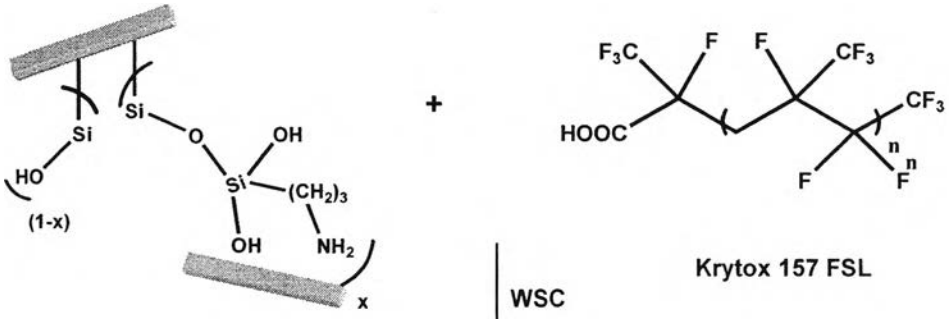

Krytox 157 FSL

WSC

Step 3

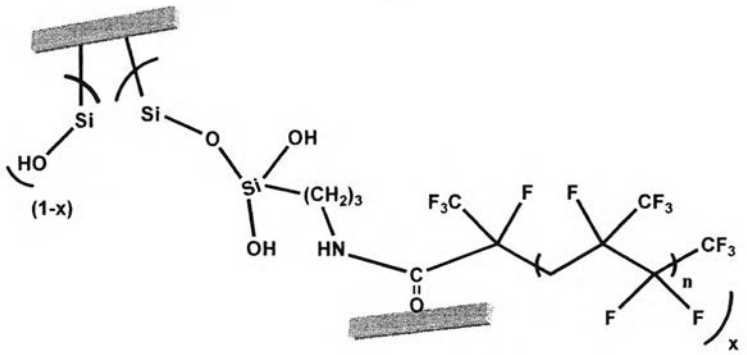

3

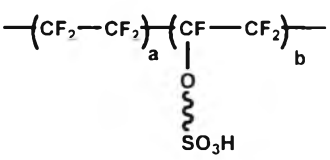

5 wt.% Nafion® solution

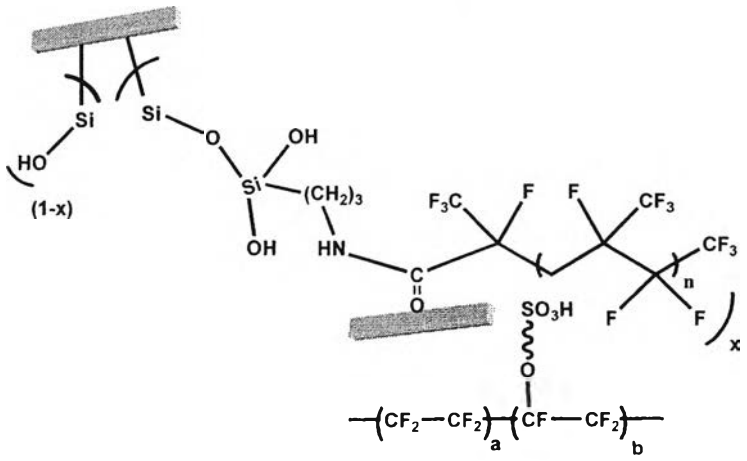

Step 4

4

The two solutions obtained (30 ml) were cast onto a Teflon mold (6 cm x 6 cm x 1 cm) and isothermally heated at 60 °C for 6 h to obtain **4a** and **4b** nanocomposite membranes containing 2.5 and 5 wt.% of **3**, respectively. The membranes were dried in vacuum oven at 80 °C for overnight and detached after soaking in water for several hours. Five percent weight of Nafion® in aliphatic alcohol solution was cast by the same procedures to obtain a recast Nafion® membrane. All membranes show a thickness of around 80 μm.

2.3. Structural characterization

The products obtained were characterized by a Thermo Nicolet Nexus 670 Fourier transform infrared (FT-IR) spectrometer and a PERKIN ELMER 2400 CHN Elemental analysis (EA).

FT-IR (KBr, cm^{-1}) for **2**: 3625 and 3435 (free and hydrogen-bonded OH, respectively), 3300 (NH_2), 2930 and 2860 (CH_2), 1632 (NH_2 bending) and 1040 (Si-O-Si).

Anal. Calcd. for **2** ($H_2N(CH_2)_3Si(OH)_2$-O-MMT) (%): C, 21.95; H, 6.10; and N, 8.54. Found: (%) C, 8.51; H, 2.95; and N, 2.37:

FT-IR for **3** (ZnSe, cm^{-1}): 3628 and 3393 (free and hydrogen-bonded OH, respectively), 3298 (NH), 2948 and 2887 (CH_2), 1785 (C=O carboxylic acid), 1653 (C=O amide I), and 1559 (NH bending coupled C-N amide II).

2.4 Dispersion and interlayer distance of MMT

The changes in interlayer distance of MMT clay layers were confirmed by X-ray diffraction (XRD) using a Rigaku RINT 2000 diffractometer (40 kV, 30 mA) with Ni-filtered Cu Kα radiation (λ=3.07 A°). X-ray data were collected from 2° to 12° (2θ) with scanning rate of 2°/min. The intensity of diffracted X-ray from the sample was measured by a scintillation counter. The interlayer distance, d, in the clay galleries was calculated by Bragg's law, $d=\lambda/2\sin\theta_{max}$, where θ_{max} is the position of the (001) peak in the XRD spectrum.

2.5. Membrane morphology

The membrane morphology was studied by an LEO 1550 VP scanning electron microscope with both secondary and back scattered electron detectors. For atomic force microscopy (AFM), the Multi Mode Scanning Probe Microscope Model with a nanoscope IV controller by Digital Instruments Inc. (Veeco Metrology

Group), Santa Barbara, CA, USA was used. The AFM observations were carried out in air at ambient conditions (25 °C) using tapping mode probes with constant amplitude. The tapping mode etched phosphorous (n) doped silicon probe (square pyramid in shape with a spring constant of 40 N/m, nominal radius of curvature of < 10 nm) with resonance frequency of approximately 300 kHz was used. Height and phase images were recorded simultaneously at the resonance frequency of the cantilever with a scan rate of 2 Hz and resolution of 512 samples per line. The scanning was done at 3 different positions for each sample.

2.6. Water uptake and thermal stability

The membranes were immersed into distilled water at 60 °C for 2 days. The water uptake was determined by thermogravimetric analysis technique using a TGA 2950 DuPont. The membrane was heated from room temperature (25 °C) to 60 °C and cooled down again to room temperature. The second heating run was started from room temperature to 700 °C. Both processes were operated with the heating rate of 10 °C/min under nitrogen atmosphere. The water content retained in the membrane was calculated from the percent weight loss of water at temperature below 250 °C. The degradation temperature was carried out at 250-700°C.

2.7 Methanol permeability measurement

The methanol permeability was determined by using a 30 ml-two-compartment glass cell as reported elsewhere [15] (Scheme 5.2). Compartment A was filled with 10 %(v/v) methanol and 1 %(v/v) ethanol while compartment B with 1 %(v/v) ethanol. The membrane was placed in between these two compartments. The sample solutions from both compartments were taken at the 90 min interval time. The methanol concentration in each solution was analyzed by gas chromatograph (GC) using a Shimadzu 7AG with Porapak-QS column at 160 °C. Methanol concentrations of all samples were determined by the proportion of the integrated peak areas of methanol versus the ethanol internal standard. The methanol permeability, P (cm^2/s), was calculated as the following equations [15]:

$$V_B \times \frac{dC_{B(t)}}{dt} = P \times (C_A - C_B) \times \frac{A}{L} \qquad (1)$$

$$C_A >> C_{B(t)}$$

$$P = \frac{V_B \times L \times \frac{dC_{B(t)}}{dt}}{C_A \times A} \quad (2)$$

where C_A and C_B are the methanol concentration in the compartments A and B (%(v/v)), respectively, t is the permeation time (s), A is the exposed area of the membrane (cm^2), L is the thickness of the membrane (cm) and V_B is the solution volume of the compartment B (30 cm^3).

Scheme 5.2 Methanol permeability measurement equipment

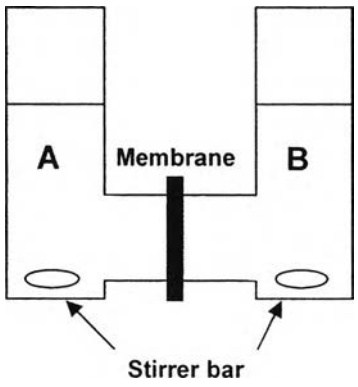

2.8. Proton conductivity measurement

Prior to the proton conductivity measurement, the membranes were soaked in 1 M H_2SO_4 at room temperature for 2 days and in distilled water at room temperature for 2 days. The proton conductivity was measured by an AC impedance spectroscopy using an IM6 Zahner Elektrik connected to a PC running electrochemical impedance software in the frequency range of 10-10^6 Hz at 40-100 °C under 100% relative humidity. The measurements were carried out on stacks containing up to three membranes resulting in cumulative thickness around 240 μm. The relative humidity was controlled by a stainless steel sealed-off cell, consisting of two cylindrical compartments connected by a tube. One compartment was filled with water while the other was housed with the membrane under test. The proton conductivity was estimated by impedance values at phase angle zero [22].

3. Results and Discussion

3.1. Fuctionalization of MMT

Figure 5.1 (a) shows the characteristic peaks at OH (3440 cm^{-1}), NH_2 (3364 and 3293 cm^{-1}) and CH_2 (2930 and 2800 cm^{-1}) stretching with NH_2 bending (1632 cm^{-1}), implying the successful hydrolyzation of (3-aminopropyl)triethoxysilane to obtain **1**. After refluxing MMT-ethanol suspension with **1**, the product obtained, **2**, shows the peaks at 3625 and 3435 cm^{-1} belonging to the free and hydrogen-bonded OH groups of MMT, a strong Si-O-Si peak at 1040 cm^{-1} while most other peaks are similar to **1** (Figure 5.1 (b)). This indicates the silylation of aminosilane onto the MMT layers. Figure 5.1 (c) shows the characteristic peaks of Krytox 157 FSL at 3100 cm^{-1} (OH), 1785 cm^{-1} (C=O), 1250 cm^{-1} (CF_3) and other peaks in the range of 1100-1400 cm^{-1} (CF). In the case of **3**, the peaks at 3298 cm^{-1} (NH stretching), 2948 and 2887 cm^{-1} (CH_2 stretching), 1785 and 1635 cm^{-1} (C=O stretching and amide I), and 1559 cm^{-1} (amide II) are identified (Figure 5.1 (d)). This confirms that the Krytox 157 FSL was introduced on the MMT layers by conjugating with aminosilane as shown in Step 3 (Scheme 5.1).

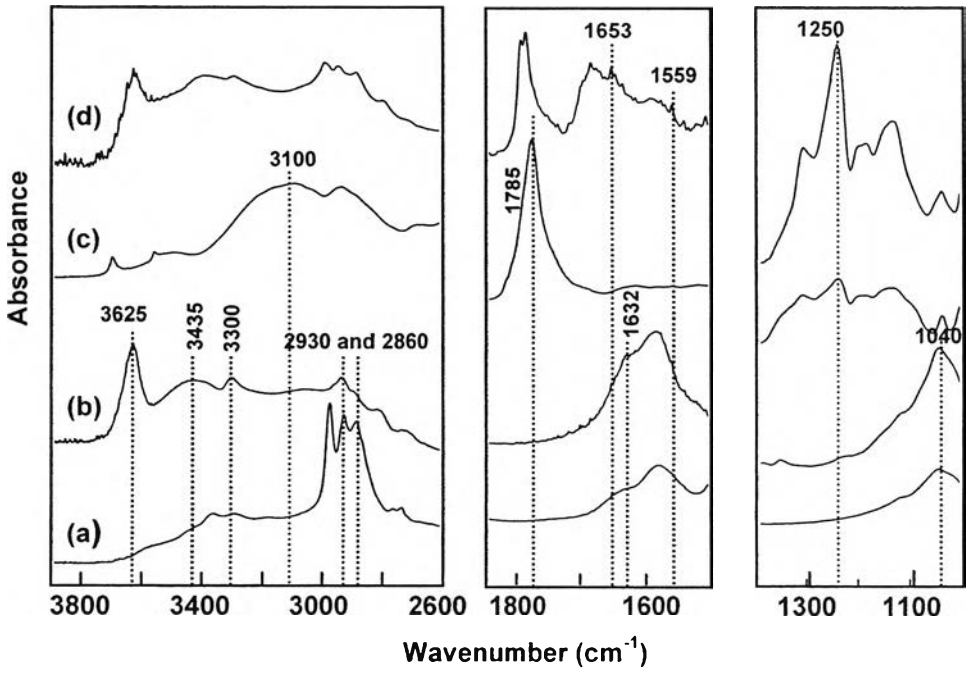

Figure 5.1 FTIR spectra of **1** (a), **2** (b), Krytox 157 FSL (c) and **3** (d).

The content of aminosilane successfully silylated onto MMT layers was quantitatively analyzed by elemental analysis (EA). The simplified structure shown as the product of Step 4 (Scheme 5.1) was assumed to calculate the substitution degree x by the equations below:

$$N(\%) = \frac{14x}{45(1-x)+164x} \times 100 \quad (3)$$

$$C(\%) = \frac{36x}{45(1-x)+164x} \times 100 \quad (4)$$

Based on the EA results, the percentage of N and C are 2.37 and 8.51, respectively. From these results the x value for 0.1 was obtained. This means that one-tenth of the OH group on MMT layers was silylated with aminosilane.

3.2. Krytox-MMT-Nafion® nanocomposite membrane

As it is known that the dispersion of nanoclay in polymer matrix is directly related to the changes in methanol, water or gas permeability through the membrane, the WAXD pattern of nanoclay in each step was analyzed. The pristine MMT shows the diffraction peak of the basal spacing (d_{001}) at 2θ=7.21° referring to the interlayer distance, d, of 12.25 Å (Figure 5.2 (a)). After the modification of MMT with aminosilane, **2** shows the characteristic peak of MMT apparently shifted to the lower 2θ angle (2θ=4.17°, 21.17 Å), indicating the aminosilane intercalation into the clay gallery (Figure 5.2 (b)). For nanocomposite membranes, **4a** and **4b**, the primary diffraction peak belonging to d_{001} basal spacing of MMT was completely disappeared (Figure 5.2 (d) and (e)). It is important to note that the diffraction patterns of **4a** and **4b** are similar to that of the recast Nafion® membrane (Figure 5.2 (c)). This implies that MMT layer was completely exfoliated with Nafion® polymer matrices. Here, we concluded that the modification of MMT layers with fluorinated polymer (Krytox 157 FSL) brings the good compatibility between MMT and Nafion® polymer matrices.

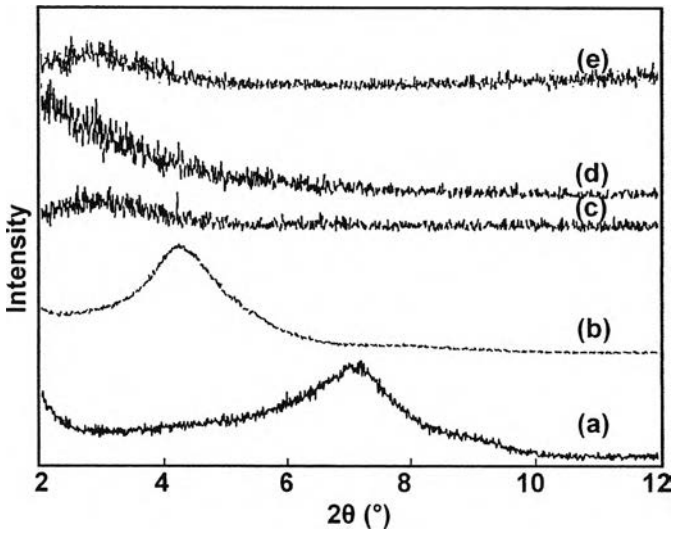

Figure 5.2 X-ray diffraction patterns of MMT (a), **2** (b), the recast Nafion® (c), **4a** (d) and **4b** (e).

3.3. Membrane morphology

The microstructures of the composite membranes were investigated by scanning electron spectroscopy. Figure 5.3 shows the homogeneous and dense membrane all over the cross sectional area of **4a** implying the well-dispersed MMT. The nano-scale exfoliation and dispersion of MMT in Nafion® polymer matrices was also supported by Figure 5.2 (d) and (e).

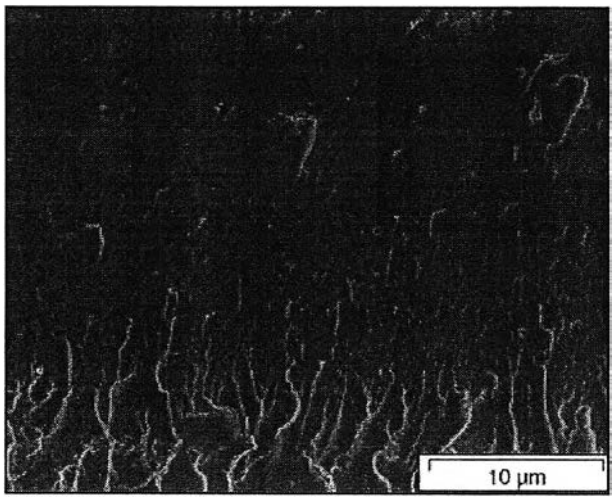

Figure 5.3 Cross-section of **4a** observed by SEM.

In addition, the morphology on nanoscale of the composite membranes was investigated by AFM. Figure 5.4 shows AFM topographic images with phase contrast. In this phase contrast mode, the effect of the topography is much smaller and the influence of other parameters, especially the difference in hardness of inorganic clay and organic polymer matrices can be clearly identified. In this case, the inorganic clay layers will give a distinct white bright area. The membrane **4a** reveals a good dispersion of **3** all over the Nafion® membrane surface (Figure 5.4 (a)). The approximate length of an individual MMT clay particle with ~ 100 nm approaching to the value reported by Maiti et al [24] is observed. In the case of **4b**, the disordered dispersion and some aggregations of individually functionalized MMT on the polymer matrices are observed (Figure 5.4 (b)). Moreover, it is important to note that the phase image of the membrane exhibits the significantly dark area surrounding each single MMT particle with an average 25 nm width which could be attributed to the Krytox (perfluoroether) chains modified onto the MMT layer surface.

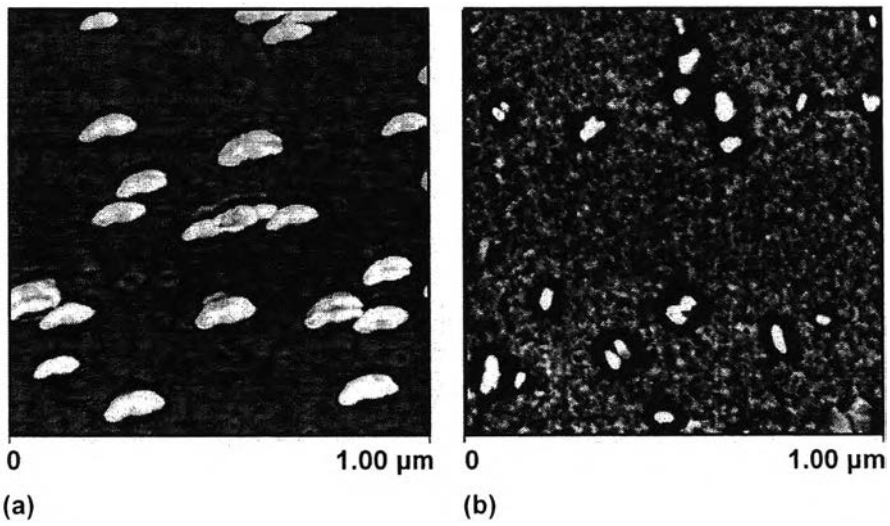

Figure 5.4 AFM topographic images of the surface of **4a** (a) and **4b** (b).

3.4. Water content and thermal stability

Since the proton conductivity and methanol permeability of the membrane are relied on microstructure, i.e., cluster and channel size [18] influenced by the amount of water absorbed in the membrane, here, the optimal water uptake is considered. To assure the water uptake of the membranes, the thermogravimetric analysis technique was carried out up to 250 °C as reported by Huang et al. [25]. From Table 5.1, it is obvious that the water uptake in the membrane is increased with **3** loading content. The recast Nafion® membrane shows a water uptake 20.8 % which is close to the value (21.6 %) reported by Li et al. [26]. The membranes **4a** and **4b** give the water weight loss 26.4 and 31.6 %, respectively. This suggested the better ability to retain water molecules in the membrane provided by the hydrophilicity of the filler. In the case of thermal stability, the recast Nafion® membrane shows the degradation (T_{d1}) attributed to the sulphonic acid moieties (-$OCF_2CF_2SO_3H$) at 296 °C and PTFE backbone (-CF_2-CF2-) (T_{d2}) at 402 °C which is close to those of Nafion® 115 membrane reported by Deng et al. [27]. For the nanocomposite membranes, the thermal decomposition curve is similar to the recast Nafion®, but the two decomposition temperatures are shifted to the higher temperature region. Moreover, the degradation temperatures are found to increase with **3** loading content, i.e., T_{d1} and T_{d2} are at 305.9 and 409.8 °C for **4a** and are at 309.8 and 417.6 °C for **4b** (Table 5.1). This could be attributed to the strong interaction between hydrophobic Nafion® backbone and organophillic clay layer [8] obtained from the exfoliation of MMT on the polymer matrices.

Table 5.1 Water uptake and degradation temperatures (T_d) of the membranes

Membranes	Water uptake (%)	T_{d1} (°C)	T_{d2} (°C)
Recast Nafion®	20.8	296	402
Nafion® 115	21.6[a]	300[b]	400[b]
4a	26.4	305.9	409.8
4b	31.6	309.8	417.6

[a] From [26]
[b] From [27].

3.5. Methanol crossover

The diffusion of methanol and water through the membranes at several intervals of permeation times was used to evaluate the methanol crossover. The experiments were conducted at 25 °C and 60 °C by using the two-compartment glass cell (Scheme 5.2) combined with GC for methanol concentration analysis. Figure 5.5 (a) shows that the methanol concentration in compartment B (C_B) increases linearly with the permeation time. Based on the slopes of such plot, for example, the values at 60 °C of 3×10^{-5}, 2×10^{-5} and 2.3×10^{-5} %(v/v) s^{-1} are achieved from the recast Nafion®, **4a** and **4b** membranes, respectively, the methanol permeability was calculated as expressed in Eq. (2). The methanol permeability at 25 °C for the recast Nafion® membrane is $8.7\text{x}10^{-6}$ cm^2/s whereas those of **4a** and **4b** are as low as $1.2\text{x}10^{-6}$ cm^2/s and $8.7\text{x}10^{-7}$ cm^2/s, respectively (Figure 5.5 (b)).

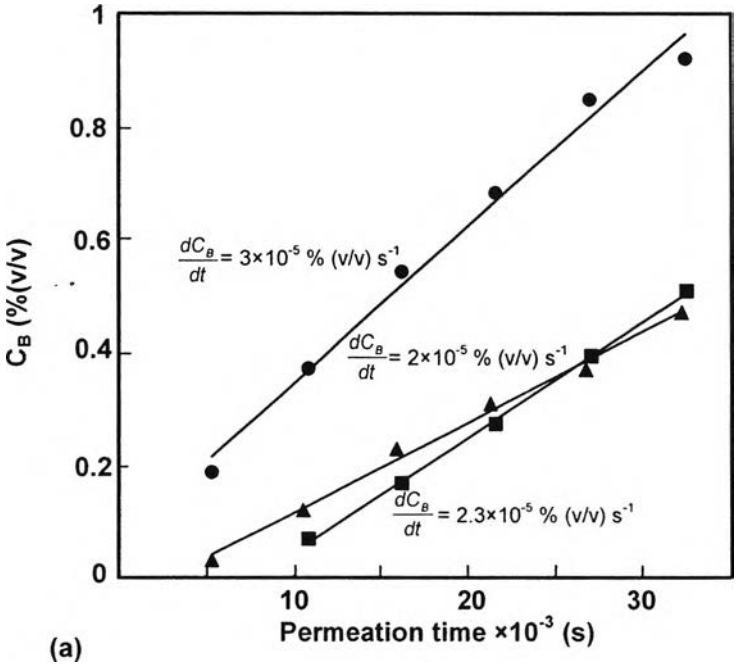

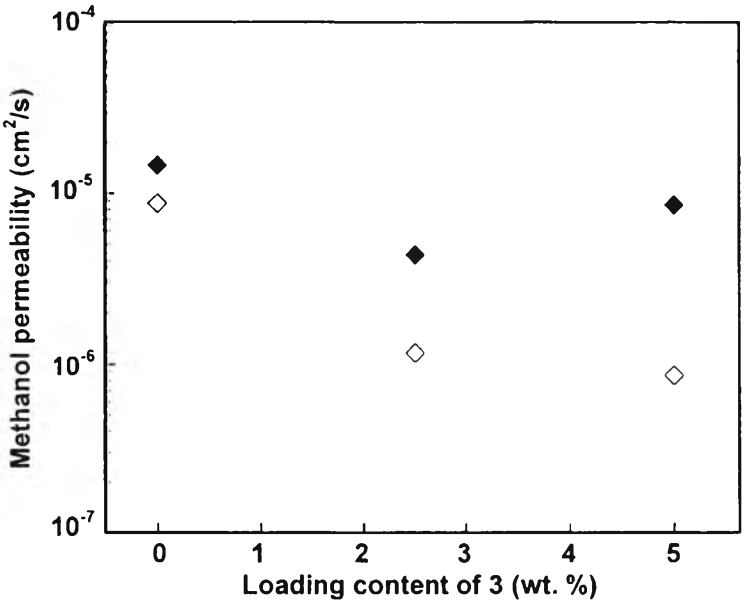

(b)

Figure 5.5 Methanol permeability of Nafion® membrane: (a) methanol concentration in compartment B (C_B) vs. permeability time at 60 °C of the recast Nafion® (●), **4a** (▲), and **4b** (■); (b) methanol permeability at 25 °C (◇) and at 60 °C (◆).

The methanol permeability at 25 °C decreases when the loading content of **3** increases. This might be due to the hindering methanol permeation of homogeneous-dispersed clay in the Nafion® polymer matrix. In addition, the significantly obstructive effect on methanol permeability was accomplished by the exfoliated pattern of the clay layers in the composite membrane. This results in the reduction of methanol permeability by a longer diffusive path based on tortuosity. The result is similar to the case reported by Gaowen et al. [23] which the significant methanol permeability reduction was obtained from the exfoliated composite membrane of sulfonated polyether ether ketone (SPEEK) and organically modified montmorillonite (OMMT) (SPEEK/OMMT). Here, we confirm that our system under an exfoliation with good dispersion of the clay layers in Nafion® polymer matrix based on the "like-dissolves-like" concept as supported from the XRD (section 3.2) and AFM (section 3.3) provides the retardation of methanol

permeability. It is important to note that the concentration of methanol also largely affects to the permeability. For example, in the case of the recast Nafion membrane, we found that the permeability was $8.7x10^{-6}$ cm^2/s in contact with 10 % (v/v) methanol solution at room temperature for the test membrane thickness 85 μm whereas that of Nafion® 117 membrane reported from Pivovar et al. [28] was $2.3x10^{-6}$ cm^2/s in contact with 4 %(v/v) methanol solution.

At 60 °C, the permeability is reduced from $1.5x10^{-5}$ to $4.3x10^{-6}$ cm^2/s independently with **3** content (Figure 5.5 (b)). It is also clear that the increase in **3** content from 2.5 to 5 wt.% hardly brings the retardation in methanol permeability. This might come from various possibilities. For example, the water uptake of sample with higher filler content could be substantially increased with temperature (60 °C), an analogously to that reported by Ren et al. [29]. This results in the high methanol permeability caused by the larger number of hydrophilic sites (-OH groups) as proposed by Deng et al. and Heizel et al. [28, 30]. Another possible reason might be due to the fact that the difference in thermal expansion at elevated temperature (60 °C) of inorganic (clay) and organic (polymer chain) parts allows the methanol permeability significantly.

3.6. Proton conductivity

The proton conductivity was studied by the AC impedance spectroscopy with various frequencies. Figure 5.6 shows an increase in proton conductivity with temperature from 40 to 100 °C under 100 % relative humidity. The proton conductivity of the recast Nafion® is in the range of 29-62 mS/cm while those of **4a** and **4b** are 25-48 and 23-32 mS/cm, respectively. Comparing the proton conductivity of Nafion® 115 membrane at 50-100 °C under 100 % relative humidity, our recast Nafion® membrane reveals lower proton conductive efficiency than that of the report by Yang et al. (100-150 mS/cm) [30]. As it is known that the membrane casting process is depended on various factors, here we carried out our own recast membrane as a reference in comparing the data of **4a** and **4b**. In the case of the nanocomposite membranes, the proton conductivity is lower than that of the recast Nafion® membrane for all temperatures, and the conductivity decreases as **3** loading content increases. Such a decrease in proton conductivity could be attributed to the blocking effect of MMT additive confining the continuum of

sulfonic acid groups of Nafion® responsible for proton conductivity which are also seen in other cases [5, 10].

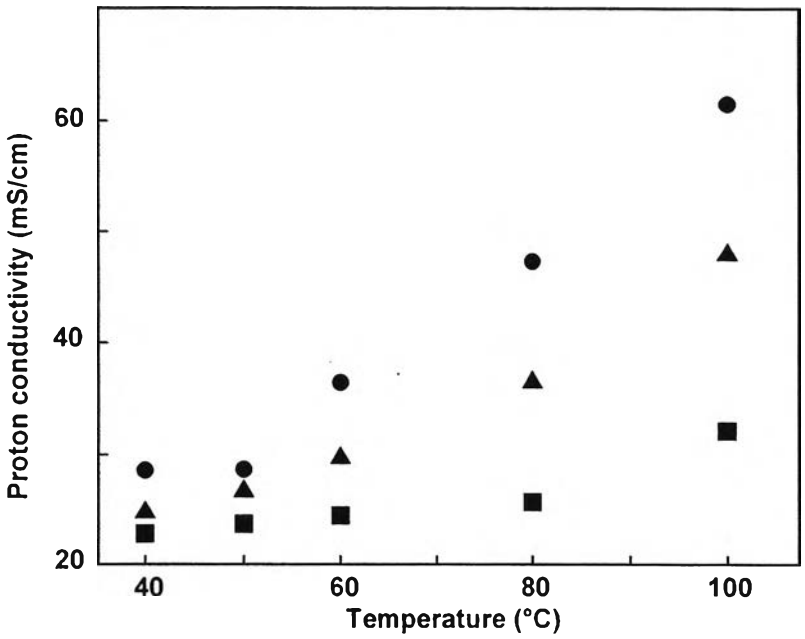

Figure 5.6 Proton conductivity of the reast Nafion® (●), **4a** (▲) and **4b** (■).

Generally, the two important parameters used to characterize the membranes in DMFC applications are the methanol permeability (P) and the proton conductivity (σ), thus, the membrane selectivity (α) defined as the σ/P ratio is considered. The logarithm of α expressed as β = log α is also another membrane selectivity evaluation [32-34]. The best DMFC performance, then, can be evaluated from the high α or β value. Here, the proton conductivity and methanol permeability at 60 °C in the range DMFC-operating temperature (25-100 °C) were considered. Table 5.2 shows that the selectivity of **4a** and **4b** are 2 and 0.6 times higher than that of the recast Nafion® membrane, respectively. Based on the membrane selectivity, it can be concluded that the best performance is obtained from the membrane containing **3** with no more than 2.5 wt.% as in the case of **4a**.

Figure 5.7 displays the Arrhenius plot of the proton conductivity as a function of temperature at 100 % relative humidity. The proton conductive activation energy (E_a) is calculated by linearly fitting the Arrhenius equation, $\sigma = \sigma_0 \exp(-E_a/RT)$. Table 5.2 shows that the E_a values decrease when the loading

content of **3** is increased. The E_a of the recast Nafion® membrane is 13 kJ/mol (0.14 eV) which is close to the reported value (10.8 kJ/mol) [23] while those of **4a** and **4b** are 11 (0.11 eV) and 5 (0.05 eV) kJ/mol, respectively. According to a Grotthus mechanism for proton migration in the polymer electrolyte membrane, the protons transfer from one solvent molecule to the other through the hydrogen bonds preferentially occurring with the E_a ranging from 0.1-0.4 eV [35].

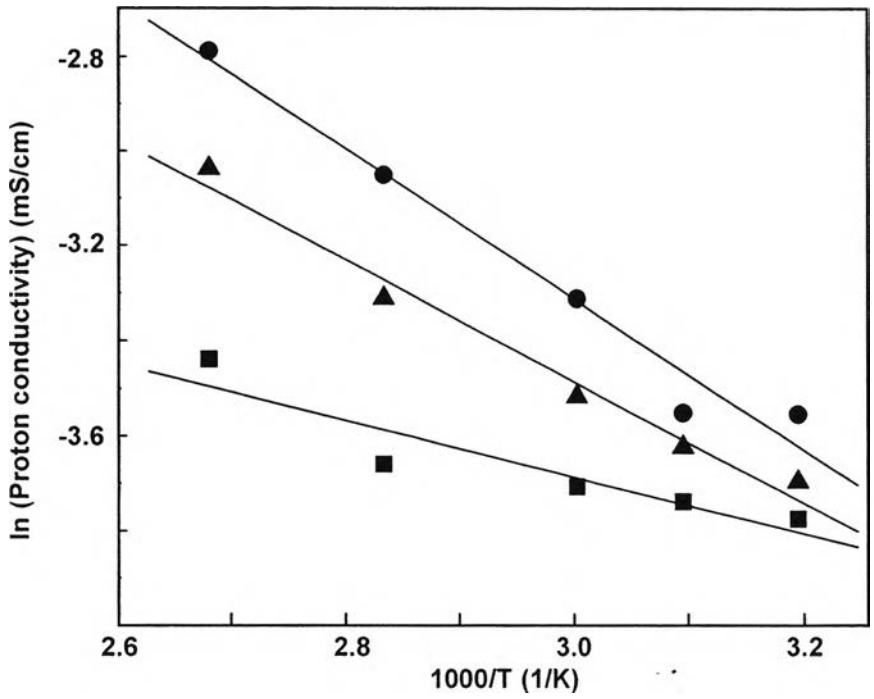

Figure 5.7 Arrhenius plot of the recast Nafion® (●), 4a (▲) and 4b (■).

Therefore, the proton migration in the recast Nafion® membrane within a preferable E_a range implied the transfer under Grotthus mechanism. In the cases of **4a** and **4b**, the E_a values are lower than that of the recast Nafion® membrane (Table 5.2) suggesting the significant efficiency for proton migration.

Table 5.2 Activation energy (E_a) and selectivity (β) of the membranes

Membranes	E_a (kJ/mol)	β (S min/cm^3)
Recast Nafion®	13	6.6
4a	11	7.1
4b	5	6.8

Combining this result with the high water uptake of **4a** and **4b** (Table 5.1), we suspect that the **4a** and **4b** membranes provide effective proton hoping along the hydrated channel. Although the proton migration of **4a** and **4b** is higher than that of the recast Nafion® membrane, we found that the proton conductivity of these membranes is lower (Figure 5.6). This might be related to several factors, such as chain mobility, the amount sulfonic acid proton conductive groups, and tortuosity. Based on the discussion in 3.2 and 3.3, we suspect that the dispersed silicate layers leads to the tortuosity which the long proton-transferring pathway is generated.

4. Conclusions

Montmorillonte (MMT) clay-layered silicate was silylated with (3-aminopropyl)triethoxysilane and further functionalized with fluoropolymer chains (Krytox 157 FSL) by using the carbodiimide conjugating agent to obtain MMT functionalized Krytox. The nanocomposite membrane was prepared by solution casting of the Krytox-MMT-Nafion®. The miscibility of the nanocomposite membrane was based on the similar structure of Krytox 157 FSL developed on the MMT layer surface and Nafion® polymer chains. The nanoclay exfoliation and the homogeneous pattern of MMT layers on the Nafion® polymer matrices were confirmed by XRD and SEM, respectively as well as the dispersion on the nanoscale of the individual MMT layer on the polymer matrices by AFM. The water retention and degradation temperature were increased when the MMT functionalized Krytox loading content was increased. The nanocomposite membranes showed as high as more than 50 % reduction in methanol permeation at 25 and 60 °C. The activation energy for proton migration was decreased with the increase in MMT functionalized Krytox content indicating an easier proton transfer in the nanocomposite membranes than in the Nafion® membrane. However, the lower proton conductivity was

obtained when the MMT functionalized Krytox loading content was increased. Considering the membrane selectivity (α or β value), the composite membranes revealed the significant DMFC performance as compared to the recast Nafion® membrane.

Acknowledgement

One of the authors acknowledged collaborative research fund of National Research Council of Thailand (NRCT) and Japan Society for Promotion of Science (JSPS), Research Task Force (Chulalongkorn University) and National Metal and Materials Technology Center (MTEC). The authors also would like to express their appreciation to M. Aderhold for the SEM pictures, as well as I. Buder for helping with the conductivity measurements. One of the authors (R. Gosalawit) would like to acknowledge the scholarship from the Institute for the Promotion of Teaching Science and Technology (IPST), Thailand.

References

[1] S.V. Andrian, J. Meusinger, J. Power Sources 91 (2000) 193.

[2] D. Kim, M.A. Scibioh, S. Kwak, I.-H. Oh, H.Y. Ha, Electrochem. Commun. 6 (2004) 1069.

[3] W. Xu, T. Lu, C. Liu, W. Xing, Electrochim. Acta 50 (2005) 3280.

[4] V. Baglio, A.S. Arico, A.D. Blasi, V. Antonucci, P.L. Antonucci, S. Licoccia, E. Traversa, F.S. Fiory, Electrochim. Acta 50 (2005) 1241.

[5] R.F. Silva, S. Passerini, A. Pozio, Electrochim. Acta 50 (2005) 2639.

[6] Y.-S. Park, Y. Yamazaki, Solid State Ionics 176 (2005) 1079.

[7] V. Tricoli, N. Carretta, M. Bartolozzi, J. Electrochem. Soc. 147 (2000) 1286.

[8] M.-K. Song, S.-B. Park, Y.-T. Kim, K.-H. Kim, S.-K. Min, H.-W. Rhee, Electrochim. Acta 50 (2004) 639.

[9] D.H. Jung, S.Y. Cho, D.H. Peck, D.R. Shin, J.S. Kim, J. Power Sources 118 (2003) 205.

[10] Y. Kim, J.S. Lee, C.H. Rhee, H.K. Kim, H. Chang, J. Power Sources 162 (2006) 180.

[11] S. Ren, G. Sun, C. Li, Z. Liang, Z. Wu, W. Jin, X. Qin, X. Yang, J. Membr. Sci. 282 (2006) 450.

[12] C. Li, G. Sun, S. Ren, J. Liu, Q. Wang, Z. Wu, H. Sun, W. Jin, J. Membr. Sci. 272 (2006) 50.

[13] Y.-S. Park, Y. Yamazaki, Eur. Polym. J. 42 (2006) 375.

[14] F. Bauer, M.W.-Porada, J. Power Sources 145 (2005) 101.

[15] R. Jiang, H.R. Kunz, J.M. Fenton, J. Membr. Sci. 272 (2006) 116.

[16] Z.X. Liang, T.S. Zhao, J. Prebhuram, J. Membr. Sci. 283 (2006) 219.

[17] Z. Liu, B.Guo, J. Huang, L. Hong, M. Han, L.M. Gan, J. Power Sources 157 (2006) 207.

[18] H.-J. Kim, Y.-G. Shul, H. Han, J. Power Sources 158 (2006) 137.

[19] K. Yano, A. Usuki, A. Okada, J. Polym. Sci. A 35 (1997) 2289.

[20] J.-M. Thomassin, C. Pagnoulle, D. Bizzari, G. Caldarella, A. Germain, R. Jerome, Solid State Ionics 177 (2006) 1137.

[21] R. Gosalawit. S. Chirachanchai, H. Manuspiya, E. Traversa, Catal. Today 118 (2006) 259.

[22] S. Vetter, B. Ruffmann, I. Buder, S.P. Nunes, J.Membr. Sci. 260 (2005) 181.

[23] Z. Gaowen, Z. Zhentao, J. Membr. Sci. 261 (2005) 107.

[24] M. Maiti, A.K. Bhowmick, Polymer 47 (2006) 6156.

[25] L.-N. Huang, L.-C. Chen, T.L. Yu, H.-L. Lin, J. Power Sources 161 (2006) 1096.L.

[26] Li, J. Zhang, Y. Wang, J. Membr. Sci. 226 (2003) 159.

[27] Q. Deng, C.A. Wilkie, R.B. Moore, K.A. Mauritz, Polymer 39 (1998) 5961.

[28] B. S. Pivovar, Y. Wang, E. L. Cussler, J. Membr. Sci. 154 (1999) 155.

[29] S. Ren, G. Sun, C. Li, S. Song, Q. Xin, X. Yang, J. Power Sources 157 (2006) 724.

[30] A. Heizel, V.M. Barragan, J. Power Sources. 84 (1999) 70.

[31] C. Yang, P. Costamagna, S. Srinivasan, J. Benziger, A.B. Bocarsly, J. Power Sources 103 (2001) 1.

[32] Y. A. Elabd, E. Napadensky, J. M. Sloan, D. M. Crawford, C. W. Walker, J. Membr. Sci. 217 (2003) 227.

[33] A. Regina, E. Fontananova, E. Drioli, M. Casciola, M. Sganappa, F. Trotta, J. Power Sources 160 (2006) 139.

[34] R. K. Nagarale, G. S. Gohil, V. K. Shahi, J. Membr. Sci. 280 (2006) 389.

[35] H. Munakata, H. Chaiba, K. Kanamura, Solid State Ionics 176 (2005) 2445.